Tetrahedron 64 (2008) 9480–9489

Contents lists available at ScienceDirect

Tetrahedron

journal homepage: www.elsevier.com/locate/tet

Molecular dynamics simulation study on the interaction of KRN 7000 and three analogues with human CD1d

Eric Hénon [a,*], Manuel Dauchez [b], Arnaud Haudrechy [a], Aline Banchet [c]

[a] Institut de Chimie Moléculaire de Reims, CNRS UMR 6229, Université de Reims Champagne-Ardenne, BP 1039, 51687 REIMS Cedex, France
[b] MEDyC, SiRMa, CNRS UMR 6237, Université de Reims Champagne-Ardenne, BP 1039, 51687 REIMS Cedex, France
[c] Department of Chemistry, Imperial College of Science Technology and Medicine, South Kensington, London SW7 2AZ, United Kingdom

ARTICLE INFO

Article history:
Received 1 May 2008
Received in revised form 17 July 2008
Accepted 18 July 2008
Available online 23 July 2008

Keywords:
KRN 7000
Ligand–protein interaction
CD1d
Molecular dynamics

ABSTRACT

Many analogues of KRN 7000, a synthetic glycolipid (α-galactosylceramide) exhibiting immuno-stimulatory activity and antitumor properties, were previously synthesized and tested in order to understand the reasons for the resulting biological activity and Th1/Th2 cytokine profile. Principles have been established for the interaction of such glycolipids with the human CD1d molecule but the exact mechanism by which different ligands with the same polar head elicit distinct biological responses remains unclear. Based on these experiments and on the available crystal structures, protein–ligand interactions are explored using molecular dynamics simulations. Hydrogen bond interactions are examined with regard to the polar group orientation. The influence of modulations on the dynamic behavior of the CD1d–glycolipid complex is addressed. Overall, our data support the mechanism by which the shortening of the α-GalCer sphingosine chain causes a significant twist of the CD1d α1 helix structure from residue Phe84 that affects the position of CD1d residues involved in the TCR recognition.

1. Introduction

KRN 7000 is a synthetic α-galactosylceramide (α-GalCer) that binds to the hydrophobic pocket of the CD1d protein and stimulates natural killer T (NKT) cells by means of T cell receptor (TCR) recognition. KRN 7000 and structural variants of this synthetic glycolipid have been the subject of many studies in the past few years. In particular, there has been considerable interest on how to best induce a selective production of cytokines. Many studies focused on analogues that differed either by stereochemistry, by carbohydrate, or by the ceramide nature. Publication[1] of the crystal structure of human CD1d crystallized with α-GalCer gave important insights on how glycolipids are loaded into CD1d and provides guidelines for the design of new therapeutic agents. More recently, Borg et al.[2] provided the first crystal structure of a human NKT TCR associated with the CD1d–α-GalCer complex, providing detailed insights into the lipid recognition by a TCR.

Reported information in the literature essentially concern the effects elicited by the glycolipid after the activation of the NKT cells.[3] KRN 7000 proved to be efficient in vivo against several cancer tumors (for example, liver and lung tumors),[4–10] against malaria,[11–13] tuberculosis,[13] and auto-immune diseases (for example, diabetes, and lupus).[14–17] Because of those activities, KRN 7000 became a very useful pharmacological agent in fundamental and therapeutic research, and recently, several phase I clinical trials in cancer research have been published.[18–22] It has been also demonstrated that mice acquire a specific immunity against the tumor after treatment with KRN 7000. In vitro, however, its cytotoxicity against those tumor cells is insignificant. In fact, KRN 7000 is not directly cytotoxic against the infected cells. KRN 7000 and other α-glycoceramides activate the immune system against tumors and rehabilitate it in order to fight against auto-immune or pathogenic diseases. α-GalCer is presented to the NKT cells via a protein, named CD1d, associated to a β2-microglobulin (β_2m). The complex is carried by antigen-presenting cells (APCs) such as dendritic cells, macrophages.[23] Upon recognition of the CD1d–glycolipid complex by the TCR, the NKT cells rapidly initiate the secretion of several cytokines, very active soluble substances involved in cellular communication. Among these cytokines, interferon-γ (INF-γ) and interleukines-4 (IL-4) involve the so-called specific Th1 (T Helper 1) and Th2 (T Helper 2) responses, respectively. After the activation cascade of other immunity cells (for example, B cells or macrophages), the Th1 response is tuned against cancer tumors while the Th2 response is involved in the treatment of auto-immune diseases (Fig. 1). KRN 7000 produces the INF-γ and IL-4 in the same quantities. For therapies, it would be very beneficial to preferentially

* Corresponding author. Tel.: +33(0)3 2691 8497; fax: +33(0)3 2691 3166.
E-mail address: eric.henon@univ-reims.fr (E. Hénon).

0040-4020/$ – see front matter © 2008 Elsevier Ltd. All rights reserved.
doi:10.1016/j.tet.2008.07.077

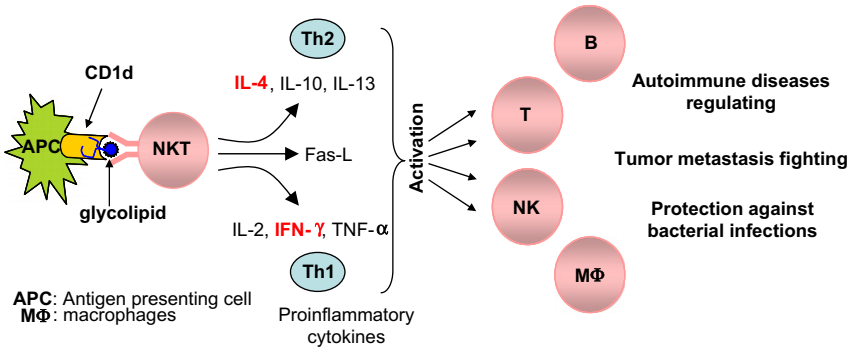

Figure 1. Activation of NKT cells by the complex CD1d–α-GalCer.

induce either response. This is the reason why so many groups work on the synthesis of analogues to favor a specific immune response.

To our knowledge, no dynamic simulations have been performed on the human CD1d–α-GalCer complex. Only a few molecular modeling studies were used to investigate specificities of the human CD1d–lipid interactions. Docking was performed by Fujio et al.[24] to model the binding of selected compounds (containing a phenyl terminal group) in the human CD1d hydrophobic pockets, and to study the interactions between these designed analogues and the protein. Their theoretical results did not vary significantly from the CD1d–α-GalCer crystal structure. In order to explain the results for short phytosphingosine analogues, Tobal et al.[25] performed a geometry optimization of the complex. They suggest that such 'static' energy calculations do not reflect the dynamics, and are not sufficient for evaluating and predicting the effects of the glycolipid modulation. A previous experimental study[26] provided useful physicochemical information about the interactions between mouse CD1d and a short chain synthetic variant of α-GalCer (PBS-25), showing the high specificity of the glycolipid as ligand.

There are at least two points to be considered in the design of new α-GalCer analogues. First, the immune response will depend on the ability of the glycolipid to be recognized by TCR. Therefore, the nature of the glycosyl head group, which is mainly involved in the recognition process,[2] is of importance. In addition, the dynamic behavior of the exposed part of the sugar bound to CD1d, and its dependence on structural variations of lipid chains should be considered as well. Moreover, the stability of the CD1d–glycolipid complex, which is mainly attributed to the length of the two lipid chains,[27] may be a contributing cause to the bioactivity. Our study of four binary complexes CD1d–glycolipid addresses these two key aspects, by characterizing the physicochemical interactions between the glycolipid and protein, and by examining the dynamic behavior of the polar head of the ligand. We performed molecular dynamic (MD) simulations of α-GalCer (AGH) and of three analogues (OCH, AGL-535, and AGP) bound to CD1d to characterize the binding of the glycolipids to the CD1d cavities. Comparisons with the X-ray structure of AGH allowed us to validate the computational methodology, and to examine the effects of structural variations on the polar head orientation and position on the recognition process. The long-term goal of our research is to rationally design ligands that induce an optimal and selective immunity response. For this, it is necessary to understand the behavior of α-GalCer in the hosting biological medium, and so it is of primary importance to give interest to physicochemical interactions with carrying cells. It is also important to address the mechanism of interaction of the glycolipid in relation with immunity system cells (essentially NKT cells).

We will use the following notation (reported in Scheme 1) for the α-GalCer ligand and its three analogues.

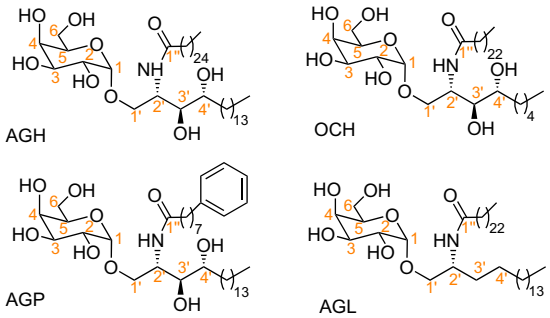

Scheme 1. α-GalCer (AGH), OCH, AGP, and AGL.

2. Results and discussions

2.1. Hydrogen-bonding interactions between α-GalCer and CD1d

The basic architecture of human CD1d was previously described.[1] It is a protein constituted of a C-terminus α3 domain, and a more complex N-terminus domain that has two α helices, which can act as a 'jaw' to hold the ligand in the active site (Fig. 2). These two helices (α1 and α2) lie on top of a seven strands β-sheet. The CD1d molecule is structurally related to major histocompatibility complex (MHC) class I molecules, except for two hydrophobic channels A′ and C′ that accommodate the two lipid chains of α-GalCer in the N-terminal part. These lipid chains consist of an acyl

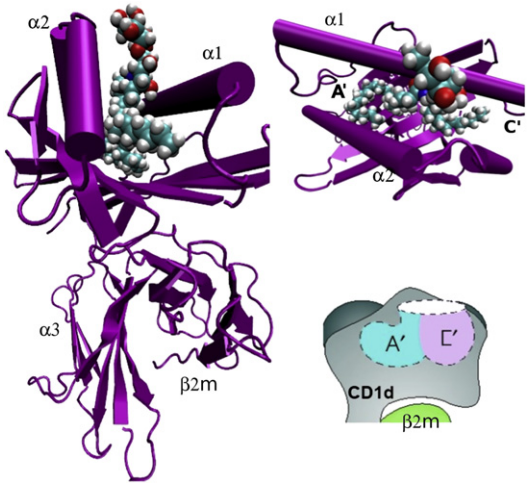

Figure 2. CD1d–α-GalCer structural features in side view (left) and orthogonal top view (right).

Table 1
Mean and standard deviation (in brackets) values of selected hydrogen bond lengths (Å) calculated during the MD simulation of four CD1d–ligand complexes

	2-OH/Asp151	3-OH/Asp151	Asp151-O/H-Thr154	Thr154-O/2′-HN	3′-OH/Asp80	4′-OH/Asp80
AGH	1.80 (0.27)	1.74 (0.27)	1.69 (0.13)	2.10 (0.18)	1.70 (0.24)	1.75 (0.37)
OCH	1.89 (0.49)	2.41 (1.40)	1.70 (0.20)	2.12 (0.22)	1.76 (0.40)	1.70 (0.33)
AGP	1.81 (0.24)	1.74 (0.27)	1.76 (0.32)	2.15 (0.24)	1.96 (0.74)	3.12 (1.37)
AGL	1.75 (0.22)	1.71 (0.17)	1.70 (0.13)	2.10 (0.22)		

Hydrogen bonds involving aspartate residues (Asp) were obtained considering the distance between hydrogen atom and the closest aspartate oxygen atom.

chain (26 carbon atoms) and a phytosphingosine chain (18 carbon atoms). In fact, α-GalCer was crystallized with two molecules of CD1d.[1] In the dimer, only one monomer contains a ligand in its active site; the non-lipid-bound monomer (empty in its active site) is placed in front of the polar head of α-GalCer. It is interesting to note that the β-sheet Gln127 residue of the lipid-free monomer H-bonds to the 4-OH hydroxyl group (with a distance of 2.61 Å between the 4-O and Gln127 N atoms), thus mimicking a receptor of the cell involved in immunological phenomena. This is in line with the recent X-ray structure[2] of a human NKT TCR in complex with a α-GalCer bound to CD1d, which revealed that the 4-position, which is free of interactions with its CD1d host, is involved in a polar recognition with the NKT cell receptor through H-bonding.

In our study, starting from the first crystal structure,[1] hydrogen-bonding interactions between the glycolipid and its host are first described from molecular dynamic simulations (see computational details in Section 4). Distances for important hydrogen bonds associated with the polar head binding as well as the sphingosine binding were monitored during the course of the MD simulation. The corresponding mean and standard deviation values are reported in Table 1. We observe that the polar head is involved in a relatively small number of intermolecular hydrogen bonds during the trajectory, as shown on Figure 3 (a snapshot taken from the molecular dynamics trajectory).

Only two interactions were clearly identified between the polar head and the CD1d α2 helix: the 2-OH and 3-OH hydroxyl groups of the D-galactose ring are hydrogen bonded to the two Asp151 oxygen atoms (mean value of 1.80 and 1.74, respectively). A full analysis of the H-bond behavior during the simulation shows that these two H-bonds remain formed even when the Asp151 carboxylate group rotates about the C–C bond after 4 ns (Fig. 4). Thereof, the orientation of the polar head between the two α helices remains unchanged during the 10 ns simulation. Actually, the sugar backbone root mean square deviation (rmsd) plot (see the AGH plot in Fig. 5) does not show significant fluctuation.

Hence, the 4-OH group always point toward the outside of the entire structure. This is in line with the experimentally found α-GalCer presentation requirements[2] shown to result from a specific H-bonding between KRN 7000 (2, 3, 4, and 3′ hydroxyl groups) and both the CDR1α and CDR3α loops of TCR (Fig. 6).

Thus, according to the X-ray structure data and to our simulation data, the 2-OH and 3-OH groups, in addition to contribute to the TCR binding, prevent the sugar head from rotating and hold the 4-OH group in a specific direction. Moreover, it is to be noted the specific position of residue Trp153 (α2) that is located in very close proximity to the exposed sugar during all the simulation (Fig. S1). Its side chain and the 'least hydrophilic' side of the sugar are in van der Waals (VDW) contact with a face-to-face configuration. The contribution of this VDW contact to the ligand binding affinity is examined in the following by means of the MM-GBSA analysis.

In other respect, detailed inspection of crystal structures[1,2] and H-bond analysis from our MD simulations do not support H-bonding between the glycosidic oxygen atom and the Thr154 (α2) hydroxyl group as previously suggested by several authors. According to the X-ray data, Thr154 can act as a H-bond donor with the glycosidic oxygen atom or a H-bond acceptor with the 2′-NH amide group. We report in Table 2 the distances and bending angles between the related heavy atoms of the Thr154 residue and AGH. In both crystal structures, the Thr154 oxygen atom is closer to the nitrogen atom than to the glycosidic oxygen atom of AGH. Moreover, the bending angles are clearly in favor of H-bonding involving the amide function rather than the glycosidic oxygen atom. In fact, the distance between the glycosidic and Thr154 oxygen atoms ranges between about 3.5 Å and 4.0 Å during all the performed dynamic simulation of the CD1d–AGH complex (mean value of 3.9 Å). Instead, it is very interesting to note that Thr154 forms hydrogen bonds both with Asp151 (α2) and 2′-NH (Fig. 7). Similarly, a previous docking model[28] of binding and recognition of glycolipids with mouse CD1d (mCD1d) suggested that the amide part of the acyl chain interacts with the Asp153 residue (equivalent to human Asp151). However, this study also suggested that Asp80 (common to mCD1d and hCD1d) interacts with the 2-OH hydroxyl group on the carbohydrate part, unlike the features pointed out by our results and by the now available crystal structures of CD1d–α-GalCer complex.

The resulting H-bond network (Fig. 3) built up from 2-*O*H, *T*hr154, *A*sp151, and 2′-*N*H (noted OTAN in the following) seems to play a central role by strongly contributing to the stability of the head group. Because the glycosidic oxygen is not H-bonded to the protein during the simulation, the binding properties of the C-analogue may be similar. These data give support to the α-*C*-galactosylceramides modulation strategy. This variation is attractive because its synthetic access is easier.[29,30] Our dynamics simulation results are consistent with the X-ray data published by Koch et al.[1] and Borg et al.[2] showing that the polar head of the α-GalCer is solely and strongly retained by the α2 helix. Molecular dynamic simulations should then provide reasonable insights into α-GalCer variations.

Turning to examine the hydrogen bonds involving the sphingosine chain of AGH we consider now the 3′-OH and 4′-OH hydroxyl groups' behavior. Previous experimental studies investigated the importance of the OH groups of the sphingosine chain. Iijima et al.,[31] using the mixed leukocyte reaction (MLR) in vitro tests, have shown that an analogue lacking the 3′-OH and 4′-OH (AGL-535) resulted in no MLR response, while the presence of the 3′-OH group alone significantly stimulated the proliferation of

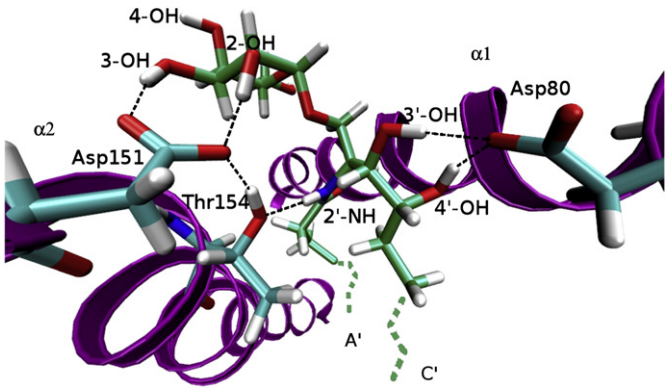

Figure 3. Hydrogen bonds network between α-GalCer (green carbon atoms) and CD1d; lipid chains are truncated for clarity; snapshot taken from the molecular dynamics trajectory.

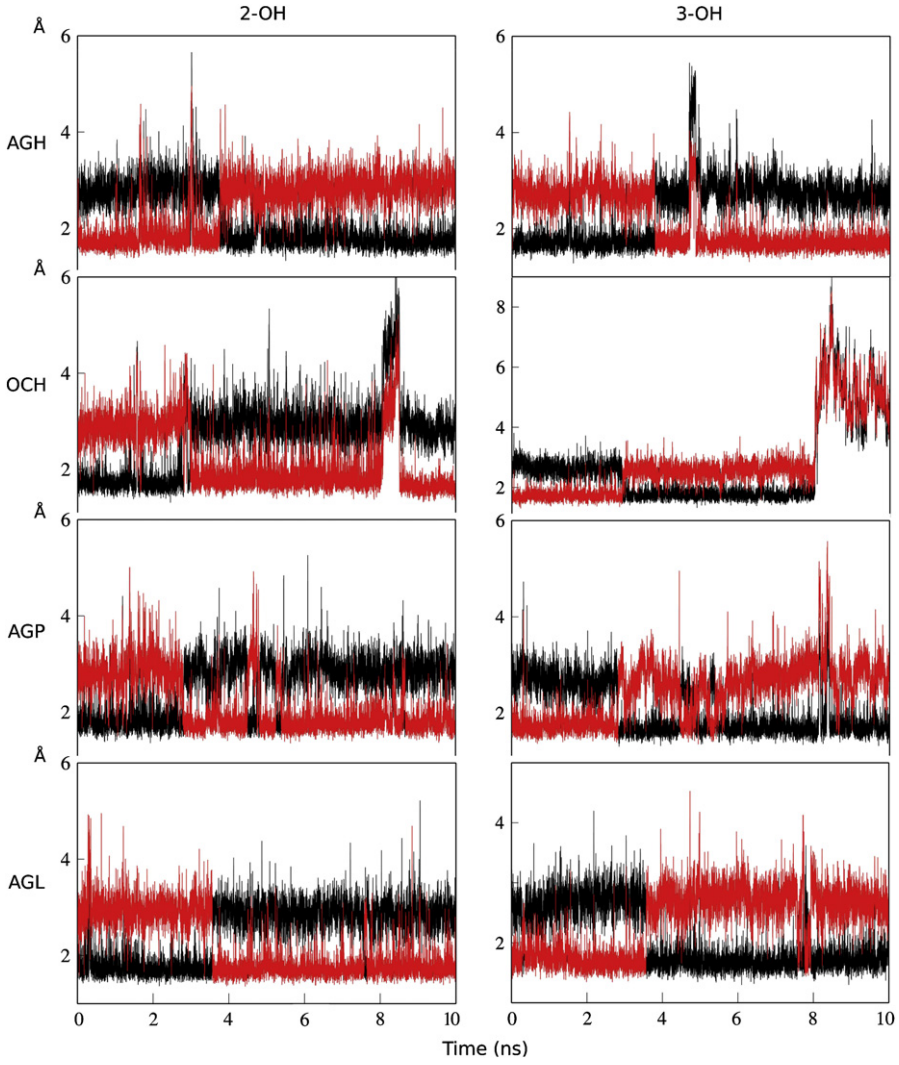

Figure 4. Hydrogen bonding between 2-OH, 3-OH, and Asp151 during a 10 ns simulation. Black and red colors refer to Asp151-O1 and -O2 oxygen atoms, respectively.

spleens cells. In parallel, Brossay et al.[32] performed tests of NKT cells reactivity to analogues presented by the human CD1d. One of their conclusions is that the presentation of α-GalCer by human CD1d to NKT cells requires the presence of the 4′-OH group, while the analogue without hydroxyl groups in positions 3′ and 4′ cannot be presented by human CD1d to NKT cells. Furthermore, 3′-OH has been found to contribute to the TCR recognition process.[2] During our simulation strong hydrogen bonding (with a distance of about 2 Å) occurs between both the 3′-OH and 4′-OH groups of the sphingosine chain and the Asp80 residue of the α1 helix (Fig. 3 and

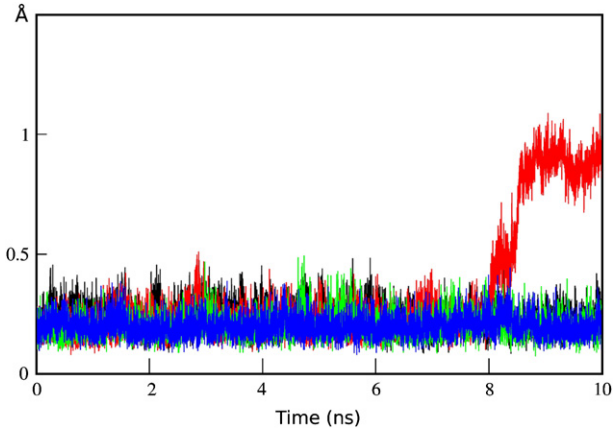

Figure 5. Polar head backbone rmsd fit between each successive structure and the first structure of the trajectory (AGH: black, OCH: red, AGP: green, AGL: blue).

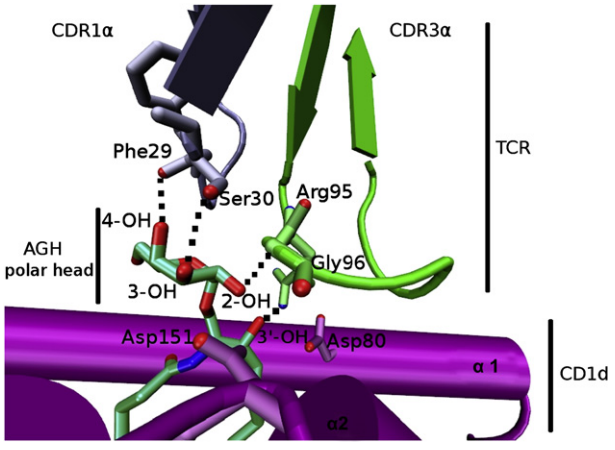

Figure 6. Selected TCR–CD1d–α-GalCer interactions from the X-ray structure by Borg et al.[2]

Table 2
Distances (Å) and bending angles (°) from the crystal structures CD1d–α-GalCer[1] (**1**) and TCR–CD1d–α-GalCer[2] (**2**)

	Crystal structure (**1**)	Crystal structure (**2**)	MD mean value (standard deviation)
Thr154 O–O Gly	2.83	3.52	3.90 (0.22)
Thr154 O–N amide	2.69	2.91	3.08 (0.17)
Thr154 C–Thr154 O–O Gly	164	170	166 (6)
Thr154 C–Thr154 O–N amide	115	125	139 (8)

'O Gly' refers to the glycosidic oxygen atom of α-GalCer; 'N amide' refers to the AGH amide function; mean and standard deviation values from the 10 ns MD of the CD1d–AGH complex are reported for comparison.

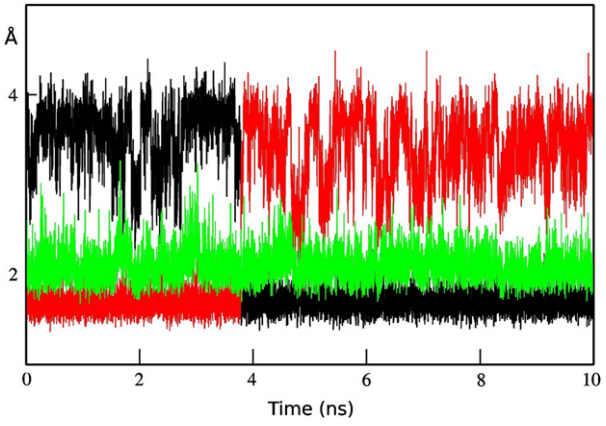

Figure 7. Hydrogen bonding between the Thr154 residue of CD1d and both 2′-NH of AGH (green) and Asp151 during a 10 ns simulation. Black and red colors refer to Asp151-O1 and -O2 oxygen atoms, respectively.

Fig. S2). From these results, hydrogen bonding involving the 3′-OH and 4′-OH groups appear to play an important role but, due to their position (after the junction of the two alkyl chains), it is not sure whether these H-bonds are related to the orientation and position of the polar head or serve to anchor the ligand into the binding groove, or both. To get insight into the role of these two hydroxyl groups, an MD simulation regarding the movement of the analogue (AGL) lacking 3′-OH and 4′-OH is presented in Section 2.2. In other respects, as suggested by Franck and Tsuji,[33] the carbonyl group of the amide function appears to be free of direct interactions with the CD1d protein. During our simulations, a water molecule bridges the carbonyl oxygen atom alternately with either the 6-OH group or the carbonyl group of Ile70 (α1), through hydrogen-bonding network. It is then relatively less exposed than the 4-OH hydroxyl group, which is directed outside the binding groove.

2.2. Comparison between α-GalCer and three analogues: polar head and lipid chains conformational flexibility

Structural variations of the polar head were performed in earlier studies,[3,31,34] but most of the analogues in the α-GalCer series derive from variations of the lipid chains.[24,31,35–38] Considerable interest has been devoted to ligand modulations able to tune the balance of the cytokine levels. The substitution of the 3′-OH and 4′-OH hydroxyl groups has been investigated in detail as well as the lipid chain length effect on the cytokine release profiles. Determining the extent to which modulations influence the cytokine release is a difficult task. Actually, numerous factors can play a role in the outcome of the NKT cell activation elicited by KRN 7000 and analogues, among those are the chemical nature of the polar head, the presentation to the TCR binding region, the ternary and binary complexes stability, the loading requirement onto CD1d (acidic pH, dependence on endosomal loading for presentation by CD1d,[36] the hydrolytic degradation of ligands by glycosidases).[39] However, principles were established from earlier studies. The length of the NKT cell stimulation by CD1d-associated glycolipids is determined by the length of the sphingosine chain, and chain-shortened glycolipids (such as the OCH analogue) seem to result in a less stable CD1d–ligand complex with a shorter half-life.[40] Since the IL-4 production was shown to require shorter TCR stimulation than IFN-γ,[40] it has been thought[24] to generate less stable CD1d–ligand complexes in order to elicit the cytokine profile toward a Th2 response. Conversely, a biased Th1 response was predicted through increasingly stable CD1d–glycolipid complexes. Furthermore, the synthesis of lipids with unsaturated bonds into the acyl chain has provided a new important clue to the understanding of the stability of the resulting complexes. Recent studies[24,36,38] (with the insertion of double bonds or a terminal aromatic group into the acyl chain) revealed that CD1d aromatic residues could be used to promote specific interactions with the glycolipid (Fig. 8).

The CD1d–ligand complex stability most certainly plays a central role in all these experiments. This key aspect can be addressed by calculating binding free energies based on MD trajectories (work in progress). But, in our opinion, the mechanism by which analogues of KRN 7000 might elicit a destabilization of the polar head or alter the position of those residues that are involved in the TCR recognition process should be considered as well. Actually, recent experiments[27] demonstrated that the sphingosine chain length solely governs the binding affinity of TCR to CD1d–glycolipid complex. In this work, a model was advanced in which the CD1d protein could undergo conformational changes issued by the modulation of the lipid chain buried in the C′ channel. A partial collapse of the unfilled portion of the pocket would result in surface-exposed structural changes modulating the TCR recognition. More precisely, the authors suggest that positional changes in the Asp151 and Thr154 residues could result from this mechanism, preventing the hydrogen network from dictating the head group position and then affecting the recognition process.

In our work, we have used molecular dynamics simulations of 10 ns duration to explore the dynamic behavior of both the sugar part and the lipid chains of three analogues (Scheme 1) bound to CD1d. The truncated sphingosine analogue (OCH, C24:9) was previously found to induce a 'Th2 biased' response,[40,41] but it also leads to a lower response than KRN 7000.[42] Furthermore, a previous experimental study, using the mixed leukocyte reaction (MLR) in vitro test, has shown that the AGL-535 analogue (no hydroxyl groups in the sphingosine chain, C24:18) results in no MLR stimulatory activity.[31] More recently, a synthesized compound bearing

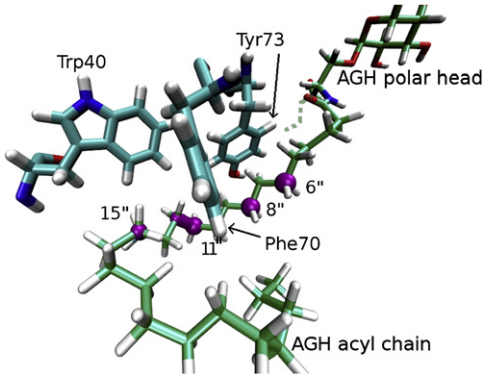

Figure 8. Location of inserted double bonds (purple cylinders at positions 11″ and 14″) and terminal phenyl (purple spheres at positions 6″, 8″, and 11″) into the acyl chain of different tested analogues. Aromatic residues Trp40, Tyr73, and Phe70 of CD1d. Carbon atoms of AGH are in green; the sphingosine chain of AGH is truncated for clarity.

a terminal phenyl group into the truncated acyl chain (C8:18) was found to be more potent than KRN 7000 with a bias for IFN-γ secretion.[35] The AGP notation has been reserved for this molecule in the following.

The influence of modulations onto the polar head orientation dynamics was first examined. As evidenced by Figure 5, removing the 3′-OH and 4′-OH groups (AGL analogue) does not destabilize the polar head orientation along the simulation, as compared with AGH. Actually, no conformational change is revealed by the sugar backbone rmsd plotted as a function of time. This result is confirmed by the OTAN hydrogen bonds network analysis for AGL (Fig. 4 and Fig. S3). One can then assume that the specific sugar orientation solely results from hydrogen bonding involving the polar head itself (2-OH and 3-OH) and the amide function (Fig. 3). As the 2-OH and 3-OH hydroxyl groups are essential for efficient recognition by TCR, a chemical alteration concerning the amide function only, without sugar modification, may be expected to impact this hydrogen bond network and might provide a way to induce a polar group destabilization and then a Th2 bias response. This is in line with the experimental results of Lee et al.[43] who have shown that one bioisosteric analogue containing an 1,2,3-triazole function in place of the amide function seems to be in favor of the Th2 immune response. A computational approach would be useful to estimate the influence of replacing the amide function.

In other respects, the truncation of the sphingosine chain (OCH) revealed very interesting features. As shown in Figures 4 and 5, the shortening of the sphingosine chain affects the positional stability of the ligand exposed part by mainly breaking the H-bond between 3-OH and Asp151 after 8 ns. The resulting new position of the head group (Fig. 9) shows H-bonding between the 6-OH group and the Arg79 (α1) residue previously shown to be involved in the recognition process through interaction with Asp94α at the CDR3α–CD1d interface.[2]

The 4-OH group orientation is then drastically altered and it is reasonable to assume that all these structural changes do not favor the binding affinity of the binary CD1d–OCH complex to TCR. The truncation of the sphingosine chain has been shown to lead to a less stable complex with CD1d,[40] but in addition, from our study, it seems that dynamic factors may play a role by hindering the TCR recognition. It is to be noted that the polar head destabilization was only observed during the dynamic simulation of the OCH analogue.

Next, we examined the influence of the sphingosine chain truncation on the α1 and α2 helices. Figure 10 represents the superposition of the lowest energy structures obtained from simulations of the AGH, OCH, and AGP ligands in complex with CD1d (AGL has been removed from the figure for clarity). Alignment was performed using a rmsd fit of the complexes (with OCH, AGP, and AGL) based on the AGH α1/α2 helices backbone. Interestingly, the lack of lipid chain, in the C′ hydrophobic channel of CD1d binding

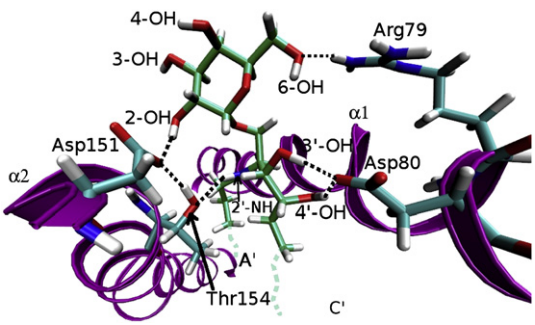

Figure 9. Hydrogen bonds network between the OCH analogue and CD1d protein after 8 ns of simulation; lipid chains of AGH are truncated for clarity.

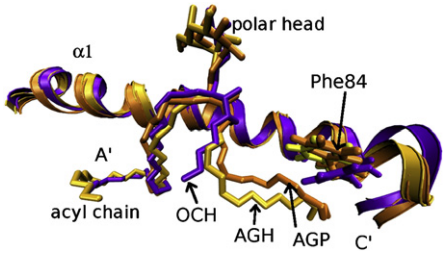

Figure 10. Lowest energy structures of the AGH, OCH, and AGP ligands in complex with CD1d from the 10 ns trajectories; alignment was to the AGH α1 and α2 helices backbone; the α2 helix and AGL–CD1d complex are removed for clarity.

the OCH analogue causes the phenyl group of the Phe84 residue (α1) to be significantly shifted down into the groove, as compared with the AGH, AGP, and AGL analogues. As a consequence, this deviation of Phe84 induces a poor structural alignment from residue 83 to the end of the α1 helix (Fig. 10). Thus, this settling induces a small but significant distortion of mainly the α1 helix that affects the residues involved in the TCR recognition mediated by CDR2β (Glu83, Lys86, Arg89). Since the Phe84 residue has been shown to make VDW contacts with the Leu99α residue of the CDR3α loop of TCR,[2] such an offset might result in reducing the interaction with the TCR α-chain. In order to confirm that this settling can be ascribed to the CD1d partially unfilled C′ pocket of CD1d bound to OCH, the Phe84 backbone rms deviation from the corresponding amino-acid of a common reference structure was calculated for the AGH, OCH, AGP, and AGL ligands bound to CD1d (see computational details in Section 4) and plotted as a function of time. As can be seen from Figure 11, the OCH analogue induces the most important deviation, as compared with the other compounds that entirely fill the C′ channel. Such a deviation was not observed for the residues of OCH before residue 83 of helix α1. Moreover, it seems that the Phe84 side chain settling occurs without impacting the OTAN H-bond network and independently of the polar head rocking motion observed from 8 ns for OCH. These results are in line with those of McCarty et al.[27] who showed that the shortening of the sphingosine chain weakens the stability of the TCR binding to CD1d–glycolipid complex.

We turn now our focus to the way the glycolipid moves within the trapping CD1d pockets noted A′ and C′. The ability of KRN 7000 to fit perfectly within the two channels A′ and C′, the length of the two chains, the curve of the acyl chain around a central pole, have been discussed in details by Koch et al.[1] The sphingosine backbone

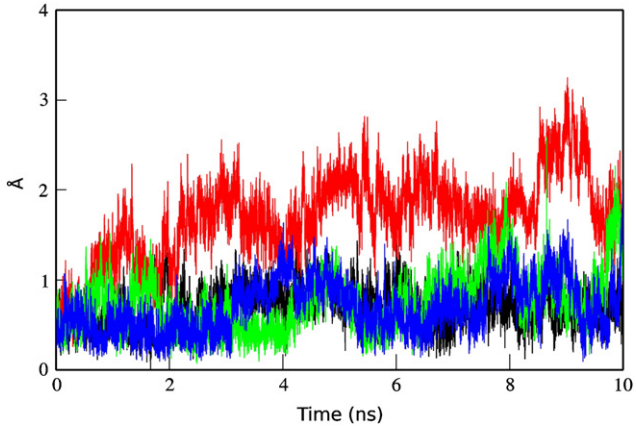

Figure 11. rmsd of the CD1d Phe84 residue backbone between each successive trajectory structure and the AGH–CD1d lowest energy structure as reference; alignment was to the AGH α1 and α2 helices backbone; AGH: black, OCH: red, AGP: green, AGL: blue.

rmsd is reported as a function of time in Figure 12 for those compounds having the same sphingosine chain length (AGH, AGP and AGL). The plot does not show excessive fluctuations and we can see the formation of several significant plateaus revealing conformations with stability from 100 ps to several nanoseconds along the simulation. Thus, despite the multitude of possible conformations of the sphingosin lipid chain (18 carbon atoms for AGH), the internal motions in the binding pocket occur with only a relatively few degrees of freedom. The acyl chain rmsd plot shows relatively more reduced fluctuations for the AGH, OCH, and AGP analogues. These findings are in line with pockets perfectly enclosing the lipid chains of the ligands. However, longer simulations and binding affinity computations are required to gain a deeper insight into the relative stability of the ligands.

An interesting variant is the introduction of an aromatic group into the acyl chain. Analyzing the position of the phenyl terminal part in the simulation of the AGP analogue we determined that the aromatic group adopts orientations to interact with the Tyr73 (α1) residue, as suggested by Fujio et al.[24] and the Phe70 (α1) residue as well (Fig. 13). Our results are in line with the author's suggestion that making specific interactions with the glycolipid could be utilized to induce a stronger Th1 response (as experimentally observed for AGP) through CD1d binding enhancement. Furthermore, according to its size (C8 for AGP), the terminal part of the acyl chain was expected to explore each side of the central pole Cys12 (β strand) during the simulation: toward the α1 helix or toward the α2 helix. Instead, as shown in Figure 13, the phenyl group is found to be continuously enclosed by three residues: Phe70, Tyr73, and Cys12, and is held in the region of the α1 helix along the simulation. In fact, Phe70 acts as a guide by attracting the lipid chain toward the α1 helix side of the A′ channel only.

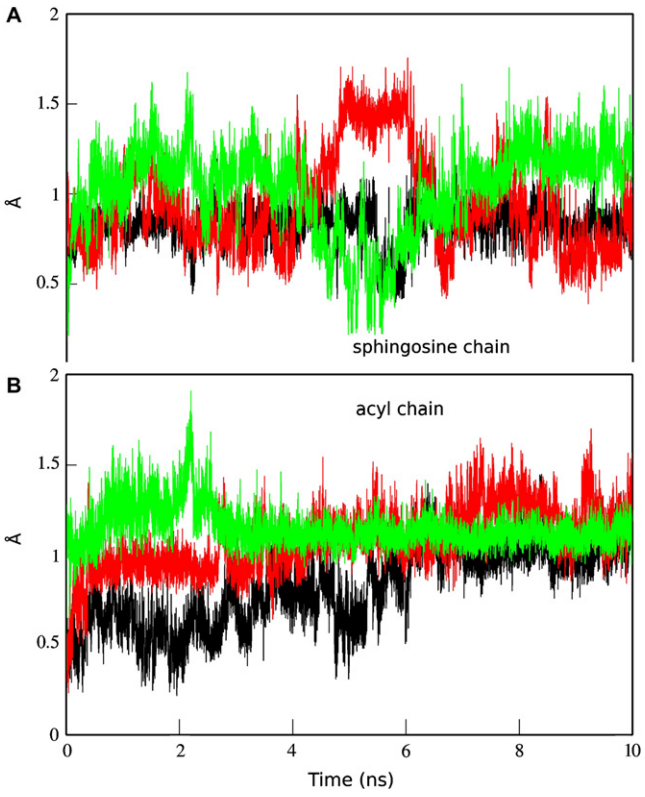

Figure 12. Glycolipid chains backbone rmsd fit between the trajectory structures and the first structure as reference (A) sphingosine, AGH: black, AGP: red, AGL: green; (B) acyl, AGH: black, OCH: red, AGL: green.

This is in line with the counter-clockwise direction observed in the crystal structure for the KRN 7000 acyl chain found to roll around the Cys12 pole.[1] This specific structural feature of the acyl chain was previously used to explain why the C20:2 analogue (KRN 7000 analogue with two Z double bonds in the acyl chain at positions 11 and 14) dissociates from CD1d more slowly than the C20:0 analogue (no double bonds).[27,36] Actually, McCarthy et al.[27] suggest that preformed curvature of the acyl chain (presence of Z double bonds at the right positions) may stabilize binding of the lipid by favoring the natural turning conformation of the acyl chain into the cavity. Furthermore, it could also favor the ligand loading requirement onto CD1d. Thus, based on entropic factors, the introduction of unsaturated bonds may be used to favor loading and fitting in the A′ channel. Figure 14 shows the calculated dihedral angle as a function of time for the C11–C12 and C14–C15 bonds in the AGH acyl chain during the 10 ns simulation. The dihedral plots are relatively flat and indicate very few conformational transitions. That confirms that the lipid chain has reduced degrees of freedom within this region of the A′ channel. However, it is to be noted that the dihedral average values (about 170° and 70°/170° for C11–C12 and C14–C15, respectively) are far from the 0° value experimentally imposed by the introduction of a Z double bond in C20:2.[27]

In fact, our AGH simulation suggests that the Z model does not fit well with the calculated dihedral angles forming the bend around Phe70 (Fig. S4) in the CD1d–AGH simulation. However, E double bonds configuration in unsaturated fats is known to promote a linear conformation. Inspection of all the C–C–C–C dihedral angles (values and fluctuations) around the circular pole during the 10 ns dynamics of AGH leads us to propose four positions at which the geometry of the Z double bond may help to introduce a bend relatively close to that found in the natural compound: C10–C11, C13–C14, C19–C20, and C22–23. Issued analogues would need to be addressed by further dynamics simulations to get a deeper insight into the resulting changes in the molecular structure of the complex. In addition, similar double bond introductions into the sphingoshine chain could be envisaged using an E double bond

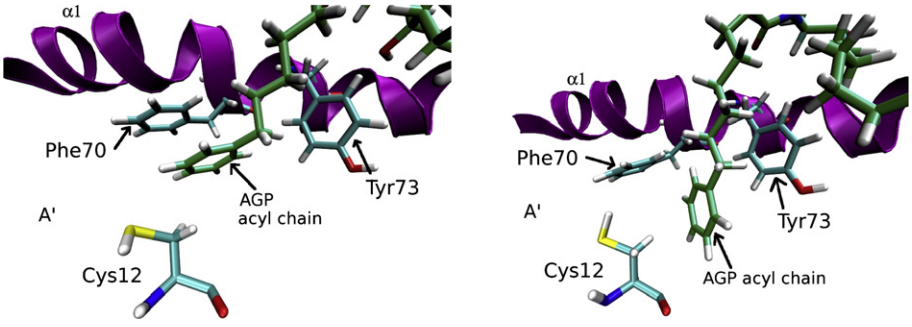

Figure 13. The two main orientations of the AGP terminal aromatic group enclosed by the Phe70, Tyr73, and Cys12 residues of the CD1d protein during a 10 ns simulation. The carbon atoms of AGP are in green.

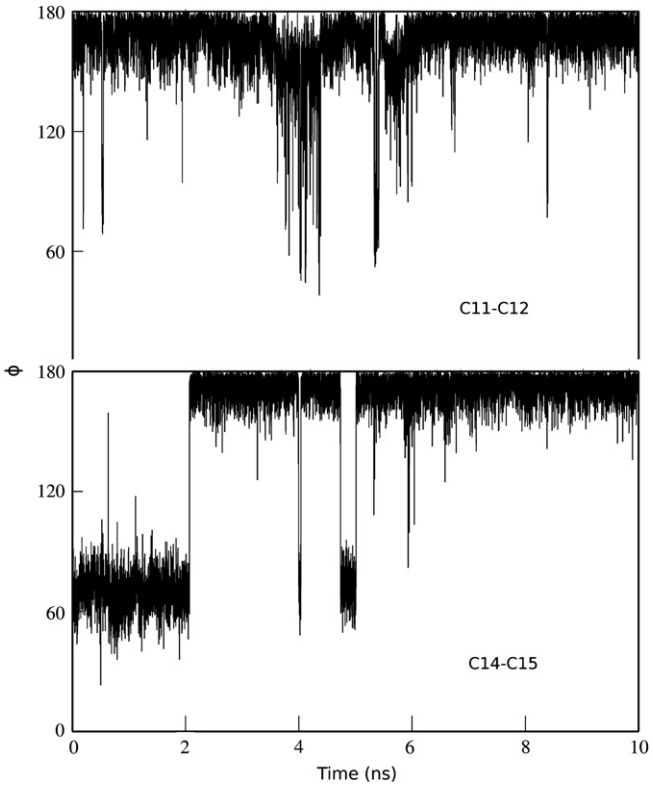

Figure 14. C–C–C–C dihedral angle Φ as a function of time for C11–C12 and C14–C15 of the α-GalCer acyl chain.

strategy due to the relative linear conformation of this chain in the KRN 7000 molecule associated with the CD1d protein. Also, it is to be noted that the two fatty chains are in very close proximity after the junction up to the carbon atoms C6″ and C8′, nearly forming VDW contacts. New modulations could account for all these structural features.

Finally, the methodology MM-PB(GB)SA (Molecular Mechanics Poisson–Boltzmann or Generalized Born Surface Area)[44] was employed to evaluate and compare the binding free energies of the four studied ligands. This approach has been thoroughly described elsewhere and compared with the potential of mean force (PMF) and thermodynamic integration (TI) methods in the frame of protein–ligand binding free energy calculations.[45,46] As can be seen in Table 3, the strongest affinity is between α-GalCer and CD1d. Investigation of the different contributions to binding (see Table S1) shows that (i) removing the 3′-OH and 4′-OH groups (AGL) results in a large decrease of the electrostatic contribution while (ii) truncating the sphingosine (OCH) or the acyl (AGP) chain results in lowering the van der Waals interaction between protein and ligand. These results, combined with the MM-GBSA per-residue decomposition analysis (see Fig. S5), confirm our previous conclusions. In particular, the residues Trp153 (VDW interaction with the carbohydrate part), Thr154 (electrostatic interaction with the amide function), and Tyr73 (VDW interaction with the acyl chain) contribute strongly to the overall binding affinity. These results also support the role of the Phe84 residue, which interacts with the untruncated sphingosine chain. On another hand, it can be noticed that the origin of the enhanced potency of the AGP ligand is still unclear and cannot be ascribed to the CD1d–AGP complex stability. Actually, the introduction of an aromatic terminal group to the truncated fatty acyl chain of AGP is found to considerably lower the overall VDW interaction and then the binding affinity. It is also to be noted that the binding energy contributions of the charged Asp80 (α1) and Asp151 (α2) residues are predicted with large standard deviations. This is because these two residues are the only to exhibit large values of the electrostatic and solvation terms, which tend to approximately cancel each other. Also, the normal mode analysis calculations present large standard deviations that introduce a significant uncertainty in the entropy contribution and then in the free energy result. Therefore, the MM-GBSA tool provides valuable insights into the nature of the binding contributions but gives relatively poor predictions for binding free energies in our case.

Table 3
Mean binding free energies ΔG (kcal mol^{-1}) of four ligands

	AGH	OCH	AGL	AGP
GB (100 snapshots)	−114.5 (4.2)	−87.1 (4.2)	−108.5 (4.8)	−78.3 (4.2)
$T\Delta S$ (10 snapshots)	−53.7 (13.4)	−32.5 (27.5)	−55.1 (20.2)	−44.9 (10.1)
ΔG	−60.8	−54.6	−53.4	−33.4

Interaction energy (GB in kcal mol^{-1}) using the generalized Born solvation model and 100 snapshots; entropy contribution $T\Delta S$ (kcal mol^{-1}) using 10 snapshots; standard deviations are in brackets.

3. Conclusion

Interaction of the KRN 7000 molecule with the human CD1d protein was explored using molecular dynamics modeling. Based on the available crystal structure of the human CD1d protein binding the glycolipid, molecular simulation trajectories of 10 ns have been used to analyze the dynamic behavior of both the sugar part and the lipid chains of α-GalCer and three analogues in complex with CD1d. Our findings suggest that the specific sugar head orientation solely results from hydrogen bonding involving the polar head itself (2-OH and 3-OH), the amide function of α-GalCer and the α2 helix. H-bond network built up from 2-OH, Thr154, Asp151, and 2′-NH strongly contributes to the stability of the head group. Thereof, we suggest that a destabilization of the exposed sugar part might be obtained by chemical modulation affecting the amide function without sugar modification. It is also to be noted that both detailed inspection of the crystal structures and the simulation data do not confirm that the glycosidic oxygen atom make hydrogen bond with the α2 helix of CD1d via the Thr154 residue. This is quite contrary to what has been earlier assumed. This result gives support to the α-*C*-galactosylceramides modulation strategy. The influence of some modulations on the dynamic behavior of the CD1d–glycolipid complex has been addressed as well. In particular, the OCH molecule (the truncated sphingosine analogue), previously found to induce a 'Th2 biased' response was studied. A polar head rocking was observed for this OCH analogue (only) after 8 ns of simulation. Structural information was obtained by examining the new position of the OCH head group after the conformational transition. In particular, the 4-OH group orientation is strongly altered and the 6-OH group forms H-bond with the Arg79 residue, which is involved in the TCR recognition process. Independently of this event, a significant settling of the Phe84 side chain of CD1d α1 helix into the binding groove was observed for OCH (only), due to the partial filling of the C′ channel of CD1d. This structural change has been found to affect the position of CD1d residues involved in the TCR recognition. Thus, in addition to the importance of the CD1d–ligand complex stability, dynamic factors may play a role by hindering TCR recognition. This aspect could be addressed by computing binding affinity of TCR to the CD1d–glycolipid complex for selected analogues. All these results are in line with the recent experimental findings of MacCarthy et al.[27] In other respects, analyzing the position of the phenyl group in the simulation of the AGP analogue associated with CD1d confirms Fujio et al.'s suggestion that CD1d aromatic residues could be used to promote specific interactions with the glycolipid.[24] However, the origin of the enhanced potency of the AGP ligand is still unclear

according to the low complex stability predicted using the MM-PB(GB)SA approach.

4. Molecular modeling

4.1. Force field parameters and generating the starting structures

All the molecular mechanics and dynamics calculations were carried out with the AMBER9[47] package. Since the present study was undertaken (September 2005) prior to the Amber9 release, the ff99 force field[48] was used for the protein instead of the ff99 Stony Brook force field modification (ff99SB),[49] which presents extremely minimal changes improving backbone torsional dihedral parameters. As stated by the authors, in addition to the overstabilization of the helical conformations present in ff99, the problem mainly originates in the inadequacy of glycine ff99 parameters. Since the α1 helix of the studied protein CD1d does not contain any glycine residue and the α2 helix contains only two glycine residues far from the glycolipid location, our simulations should allow for the comparison of CD1d host–ligand interactions for different ligands. The water molecules were modeled using the TIP3P energy function.[50] The general amber force field (gaff)[51] was used in conjunction with the antechamber program[52] (atomic charges) to describe the glycolipid. The AM1-BCC[53] charge model used by antechamber produces atomic charges that emulates the HF/6-31G* electrostatic potential of the molecule by using AM1 calculations (including a geometry optimization) and parameterized bond charge corrections. The gaff force field was preferred to the Glycam force field[54] developed for MD of glycoprotein and oligosaccharides. The published X-ray structure (PDB code 1ZT4) consists of a heavy chain loaded with α-GalCer and a β2-microglobulin (β_2m) light chain[1] that provided the initial coordinates. Hydrogen atoms were added to the ligand X-ray structure using the babel package.[55] Three disulfide bond linkages between cysteine residues have been activated as defined into the published X-ray structure. The protonation state of ionizable sidechains was examined using the very fast empirical method implemented in the Propka[56] application. Residues aspartate, cysteine, histidine, and glutamate, close to the glycolipid, received particular attention. However, the predicted pK_a shifts don't lead to a change in protonation state at physiological pH. The OCH, AGP, and AGL analogues were derived from this initial set of coordinates. The complex was explicitly solvated in a 37 Å radius sphere centered on the center of mass of the ligand (a cap of water molecules was added). The sphere is of sufficient size as to contain several layers of solvent molecules. No implicit solvent model was used beyond the solvent cap. This approach was selected because it involves fewer water molecules than a full periodic boundary treatment. Those protein atoms more than 37 Å from the cap center were restrained during the MD simulations by using a harmonic potential with a force constant of 10 kcal/(mol Å^2). These restraints include a part of the β_2m and the α3 domain. A cutoff of 15.0 Å was used for non-bonded interactions. At first, the energy of the water molecules was minimized with 500 cycles of steepest descent followed by 3500 cycles of conjugate gradient minimization during, which all of the atoms of the ligand and the protein were kept frozen. This was followed by energy minimization of the entire system, using the same protocol.

4.2. Molecular dynamics details

The molecular dynamics simulations employed a 1 fs integration time step. The water molecules were first heated from 0 to 300 K during 10 ps by the weak-coupling algorithm with a time constant for heat bath coupling of τ=1.0 ps, equilibrated for 30 ps, and then cooled to 0 K during 10 ps. During these simulations the rest of the structure was kept restrained. Next, the solvated structure (within the sphere) was heated to 300 K in 10 ps and equilibrated for a further 30 ps followed by 10 ns of data collection. rmsd fit based on sugar backbone (without 6-O) and on O–C′1–C′2(N)–C′3 backbone was employed to measure the polar head fluctuation. Similar rmsd fits were carried out to measure how much the acyl and sphingosine chains structure change during the simulations. Measure of the Phe84 residue backbone rms deviation (Fig. 11) was obtained as follows for each compound (AGH, OCH, AGP, and AGL): (1) based on the α1/α2 helices backbone selection, trajectory was aligned to the CD1d–AGH lowest energy structure, (2) the rmsd of the Phe84 backbone between each successive trajectory structure and the CD1d–AGH lowest energy structure was then calculated and plotted as a function of time.

4.3. MM-PB(GB)SA calculations

The postprocessing method MM-PB(GB)SA was used to evaluate the binding free energy of the ligand L (AGH, OCH, AGP, or AGL) to the protein CD1d (P) computed as: $\Delta G(L+P\rightarrow C)=\Delta G^{gas}(L+P\rightarrow C)+\Delta G^{solv}(C)-\Delta G^{solv}(L)-\Delta G^{solv}(P)$, where ΔG^{gas} represents the binding free energy calculated in the gas phase, and the terms ΔG^{solv} correspond to solvation free energies. The details of the calculation for the individual contributions are described elsewhere.[44] Both Poisson–Boltzmann (PB) and Generalized Born methods (GB) were employed using either 25 or 50 or 100 snapshots to confirm the GB values for the solvation electrostatic component. Only the GB method with 100 snapshots was retained for subsequent calculations. Since performing normal mode analysis is computationally expensive, only 10 snapshots were used to estimate the entropy contribution. As expected, the results show that the larger the ligand the larger in magnitude $T\Delta S$. Only a select number of residues (residues 6–184) were chosen to perform the energy decomposition presented in Table S1. This selection accounts for more than 99.7% of the total interaction energy. Solvent accessible surface area was computed using the ICOSAhedra method. Other GB input parameters are the GB model (IGB=2), the mobile counter ions concentration (saltcon=0.0), solvent (80.0) and interior of molecule (1.0) dielectric constants, and values used to compute the non-polar contribution (surften=0.0072, surfoff=0.0).

Acknowledgements

The ROMEO computational center of the University of Reims Champagne-Ardenne (http://romeo2.univ-reims.fr) and the C.R.I.H.A.N computing center (http://www.crihan.fr) are acknowledged for the CPU time donated. We thank Professor F. Bohr for reading the paper and furnishing useful comments, as well as N. Belloy for his assistance in data analysis work. We are grateful to Dr. Arjan van der Vaart for linguistic improvement of this manuscript.

Supplementary data

Figure S1 (molecular graphics), Figure S2 (hydrogen bonding plots), Figure S3 (hydrogen bonding plots), Figure S4 (dihedral angles plots), Figure S5 (MM-GBSA per-residue decomposition) and Table S1 (individual contributions to the binding interaction energy). Supplementary data associated with this article can be found, in the online version, at doi:10.1016/j.tet.2008.07.077.

References and notes

1. Koch, M.; Stronge, V. S.; Shepherd, D.; Gadola, S. D.; Mathew, B.; Ritter, G.; Fersht, A. R.; Besra, G. S.; Schmidt, R. R.; Jones, E. Y.; Cerundolo, V. *Nat. Immunol.* **2005**, *6*, 819.
2. Borg, N. A.; Wun, K. S.; Kjer-Nielsen, L.; Wilce, M. C. J.; Pellicci, D. G.; Koh, R.; Besra, G. S.; Bharadwaj, M.; Godfrey, D. I.; McCluskey, J.; Rossjohn, J. *Nature* **2007**, *448*, 44.
3. Yu, K. O. A.; Porcelli, S. A. *Immunol. Lett.* **2005**, *100*, 42.
4. Nakagawa, R.; Motoki, K.; Ueno, H.; Iijima, R.; Nakamura, H.; Kobayashi, E.; Shimosaka, A.; Koezuka, Y. *Cancer Res.* **1998**, *58*, 1202.
5. Nakagawa, R.; Serizawa, I.; Motoki, K.; Sato, M.; Ueno, H.; Iijima, R.; Nakamura, H.; Shimosaka, A.; Koezuka, Y. *Oncol. Res.* **2000**, *12*, 51.
6. Fuji, N.; Ueda, Y.; Fujiwara, H.; Toh, T.; Yoshimura, T.; Yamagishi, H. *Clin. Cancer Res.* **2000**, *6*, 3380.
7. Kobayashi, E.; Motoki, K.; Uchida, T.; Fukushima, H.; Koezuka, Y. *Oncol. Res.* **1995**, *7*, 529.
8. Kawano, T.; Cui, J.; Koezuka, Y.; Toura, I.; Kaneko, Y.; Sato, H.; Kondo, E.; Harada, M.; Koseki, H.; Nakayama, T. *Proc. Natl. Acad. Sci. U.S.A.* **1998**, *95*, 5690.
9. Cretney, E.; Takeda, K.; Yagita, H.; Glaccum, M.; Peschon, J. J.; Smyth, M. J. *J. Immunol.* **2002**, *168*, 1356.
10. Hayakawa, Y.; Rovero, S.; Forni, G.; Smyth, M. J. *Proc. Natl. Acad. Sci. U.S.A.* **2003**, *100*, 9464.
11. Hansen, D. S.; Siomos, M.-A.; de Koning-Ward, T.; Buckingham, L.; Crabb, B. S.; Schofield, L. *Eur. J. Immunol.* **2003**, *33*, 2588.
12. Gonzalez-Aseguinolaza, G.; Van Kaer, L.; Bergmann, C. C.; Wilson, J. M.; Schmeig, J.; Kronenberg, M.; Nakayama, T.; Taniguchi, M.; Koezuka, Y.; Tsuji, M. *J. Exp. Med.* **2002**, *195*, 617.
13. Chackerian, A.; Alt, J.; Perera, V.; Behar, S. M. *Infect. Immun.* **2002**, *70*, 6302.
14. Singh, A. K.; Yang, J.-Q.; Parekh1, V. V.; Wei1, J.; Wang, C.-R.; Joyce1, S.; Singh, R. R.; Van Kaer, L. *Eur. J. Immunol.* **2005**, *35*, 1143.
15. Duarte, N.; Stenstrom, M.; Sampino, S.; Bergman, M.-L.; Lundholm, M.; Holmberg, D.; Cardell, S. L. *J. Immunol.* **2004**, *173*, 3112.
16. Hong, S.; Wilson, M. T.; Serizawa, I.; Wu, I.; Singh, N.; Naidenko, O. V.; Miura, T.; Haba, T.; Scherer, D. C.; Wei, J.; Kronenberg, M.; Koezuka, Y.; Van Kaer, L. *Nat. Med.* **2001**, *7*, 1052.
17. Falcon, M.; Facciotti, F.; Ghidoli, N.; Monti, P.; Olivieri, S.; Zaccagnino, L.; Bonifacio, E.; Casorati, G.; Sanvito, F.; Sarvetnick, N. *J. Immunol.* **2004**, *172*, 5908.
18. Giaccone, G.; Punt, C. J. A.; Ando, Y.; Ruijter, R.; Nishi, N.; Peters, M.; von Blomberg, B. M. E.; Scheper, R. J.; van der Vliet, H. J. J.; van den Eertwegh, A. J. M.; Roelvink, M.; Beijnen, J.; Zwierzina, H.; Pinedo, H. M. *Clin. Cancer Res.* **2002**, *8*, 3702.
19. Nieda, M.; Okai, M.; Tazbirkova, A.; Lin, H.; Yamaura, A.; Ide, K.; Abraham, R.; Juji, T.; Macfarlane, D. J.; Nicol, A. J. *Blood* **2004**, *103*, 383.
20. Uchida, T.; Horiguchi, S.; Tanaka, Y.; Yamamoto, H.; Kunii, N.; Motohashi, S.; Taniguchi, M.; Nakayama, T.; Okamoto, Y. *Cancer Immunol. Immunother.* **2008**, *57*, 337.
21. Godfrey, D. I.; Kronenberg, M. *J. Clin. Invest.* **2004**, *114*, 1379.
22. Veldt, B. J.; van der Vliet, H. J. J.; von Blomberg, B. M. E.; van Vlierberghe, H.; Gerken, G.; Nishi, N.; Hayashi, K.; Scheper, R. J.; de Knegt, R. J.; van den Eertwegh, A. J. M.; Janssen, H. L. A.; van Nieuwkerk, C. M. J. *J. Hepatol.* **2007**, *47*, 356.
23. Moody, B. B. *Nat. Rev. Immunol.* **2005**, *5*, 387.
24. Fujio, M.; Wu, D.; Garcia-Navarro, R.; Ho, D. D.; Tsuji, M.; Wong, C.-H. *J. Am. Chem. Soc.* **2006**, *128*, 9022.
25. Toba, T.; Murata, K.; Nakanishi, K.; Takahashi, B.; Imajo, S.; Yamamura, T.; Miyake, S.; Annoura, H. *Bioorg. Med. Chem. Lett.* **2007**, *17*, 2781.
26. Zajonc, D. M.; Cantu, C.; Mattner, J.; Zhou, D.; Savage, P. B.; Bendelac, A.; Wilson, I. A.; Teyton, L. *Nat. Immunol.* **2005**, *6*, 810.
27. McCarthy, C.; Shepherd, D.; Fleire, S.; Stronge, V. S.; Koch, M.; Illiarionov, P. A.; Bossi, G.; Salio, M.; Denkberg, G.; Reddington, F.; Tarlton, A.; Reddy, B. G.; Schmidt, R. R.; Reiter, Y.; Griffiths, G. M.; van der Merwe, P. A.; Besra, G. S.; Jones, E. Y.; Batista, F. D.; Cerundolo, V. *J. Exp. Med.* **2007**, *204*, 1131.
28. Kamada, N.; Iijima, H.; Kimura, K.; Harada, M.; Shimizu, E.; Motohashi, S.; Kawano, T.; Shinkai, H.; Nakayama, T.; Sakai, T.; Brossay, L.; Kronenberg, M.; Taniguchi, M. *Int. Immunol.* **2001**, *13*, 853.
29. Guillarme, S.; Haudrechy, A. *Tetrahedron Lett.* **2005**, *46*, 3175.
30. Guillarme, S.; Plé, K.; Haudrechy, A. *J. Org. Chem.* **2006**, *71*, 1015.
31. Iijima, H.; Kimura, K.; Sakai, T.; Uchimura, A.; Shimizu, T.; Ueno, H.; Natori, T.; Koezuka, Y. *Bioorg. Med. Chem.* **1998**, *6*, 1905.
32. Brossay, L.; Naidenko, O.; Burdin, N.; Matsuda, J.; Sakai, T.; Kronenberg, M. *J. Immunol.* **1998**, *161*, 5124.
33. Franck, R. W.; Tsuji, M. *Acc. Chem. Res.* **2006**, *39*, 692.
34. Tashiro, T.; Nakagawa, R.; Hirokawa, T.; Inoue, S.; Watarai, H.; Taniguchi, M.; Mori, K. *Tetrahedron Lett.* **2007**, *48*, 3343.
35. Goff, R. D.; Gao, Y.; Mattner, J.; Zhou, D.; Yin, N.; Cantu, C.; Teyton, L.; Bendelac, A.; Savage, P. B. *J. Am. Chem. Soc.* **2004**, *126*, 13602.
36. Yu, K. O. A.; Im, J. S.; Molano, A.; Dutronc, Y.; Illarionov, P. A.; Forestier, C.; Fujiwara, N.; Arias, I.; Miyake, S.; Yamamura, T.; Chang, Y.-T.; Besra, G. S.; Porcelli, S. A. *Proc. Natl. Acad. Sci. U.S.A.* **2005**, *102*, 3383.
37. Ndonye, R. M.; Izmirian, D. P.; Dunn, M. F.; Yu, K. O. A.; Porcelli, S. A.; Khurana, A.; Kronenberg, M.; Richardson, S. K.; Howell, A. R. *J. Org. Chem.* **2005**, *70*, 10260.
38. Chang, Y.-J.; Huang, J.-R.; tsai, Y.-C.; Hung, J.-T.; Wu, D.; Fujio, M.; Wong, C.-H.; Yu, A. L. *Proc. Nat. Acad. Sci. U.S.A.* **2007**, *104*, 10299.
39. Lu, X.; Song, L.; Metelitsa, L. S.; Bittman, R. *ChemBioChem* **2006**, *7*, 1750.
40. Oki, S.; Chiba, A.; Yamamura, T.; Miyake, S. *J. Clin. Invest.* **2004**, *113*, 1631.
41. Miyamoto, K.; Miyake, S.; Yamamura, T. *Nature* **2001**, *413*, 531.
42. Stanic, A. K.; Shashidharamurthy, R.; Bezbradica, J. S.; Matsuki, N.; Yoshimura, Y.; Miyake, S.; Choi, E. Y.; Schell, T. D.; Kaer, L. V.; Tevethia, S. S.; Roopenian, D. C.; Yamamura, T.; Joyce, S. *J. Immunol.* **2003**, *171*, 4539.
43. Lee, T.; Cho, M.; Ko, S.-Y.; Youn, H.-J.; Baek, D. J.; Cho, W.-J.; Kang, C.-Y.; Kim, S. *J. Med. Chem.* **2007**, *50*, 585.
44. Kollman, P. A.; Massova, I.; Reyes, C.; Kuhn, B.; Huo, S.; Chong, L.; Lee, M.; Lee, T.; Duan, Y.; Wang, W.; Donini, O.; Cieplak, P.; Srinivasan, J.; Case, D. A.; Cheatham, T. E., III. *Acc. Chem. Res.* **2000**, *33*, 889.
45. Wang, W.; Kollman, P. A. *Proc. Natl. Acad. Sci. U.S.A.* **2001**, *98*, 14937.
46. Charlier, L.; Nespoulous, C.; Fiorucci, S.; Antonczak, S.; Golebiowski, J. *Phys. Chem. Chem. Phys.* **2007**, *9*, 5761.
47. Case, D. A.; Darden, T. A.; Cheatham, T. E.; Simmerling, C. L.; Wang, J.; Duke, R. E.; Luo, R.; Merz, K. M.; Pearlman, D. A.; Crowley, M.; Walker, R. C.; Zhang, W.; Wang, B.; Hayik, S.; Roitberg, A.; Seabra, G.; Wong, K. F.; Paesani, F.; Wu, X.; Brozell, S.; Tsui, V.; Gohlke, H.; Yang, L.; Tan, C.; Mongan, J.; Hornak, V.; Cui, G.; Beroza, P.; Mathews, D. H.; Schafmeister, C.; Ross, W. S.; Kollman, P. A. *AMBER version 9*; University of California: San Francisco, CA, 2006.
48. Wang, J. M.; Cieplak, P.; Kollman, P. A. *J. Comput. Chem.* **2000**, *21*, 1049.
49. Hornak, V.; Abel, R.; Okur, A.; Strockbine, B.; Roitberg, A.; Simmerling, C. *Proteins: Struct., Funct., Bioinf.* **2006**, *65*, 712.
50. Jorgensen, W. L.; Chandrasekhar, J.; Madura, J. D.; Impey, R. W.; Klien, M. L. *J. Chem. Phys.* **1983**, *79*, 926.
51. Wang, J.; Wolf, R. M.; Caldwell, J. W.; Kollamn, P. A.; Case, D. A. *J. Comput. Chem.* **2004**, *25*, 1157.
52. Wang, J.; Wang, W.; Kollman, P. A.; Case, D. A. *J. Mol. Graphics Modell.* **2006**, *25*, 247.
53. Jakalian, A.; Bush, B. L.; Jack, D. B.; Bayly, C. I. *J. Comput. Chem.* **2000**, *21*, 132.
54. Woods, R. J.; Dwek, R. A.; Edge, C. J. *J. Phys. Chem.* **1995**, *99*, 3832.
55. The Open Babel Package, version 2.0.0, http://openbabel.sourceforge.net/.
56. Li, H.; Robertson, A. D.; Jensen, J. H. *Proteins* **2005**, *61*, 704.